Contents

List of Figures

List of Tables

 introduction/introduction.tex

1 The ATLAS detector

"Potentielle citation sans aucun rapport avec le sujet"

— Personne inconnue, *contexte à déterminer*

1.1 General description and layout

ATLAS experiment is a multipurpose detector at the Large Hadron Collider (LHC) built, along with its peer Compact Muon Solenoid (CMS), in order to probe the p-p, A-A and p-A collisions using the full LHC luminosity [1]. Being the largest (but not the heaviest) detector ever built for a collider experiment the ATLAS detector comprises 44m in length, 25m in height and weights 7000 tonnes.
The detector has a cylindrical shape and is an onion-like arrangement of several detector systems centered at the Interaction Point (IP) as shown in fig. 11. The sub-detectors operate in the magnetic field created by the solenoid and toroid magnets (ATLAS owes its name to the latter). Data acquisition and recording is controlled by the Trigger and Data Acquisition (TDAQ) systems, allowing eventually to lower the event rate to a value, acceptable for the data storage [2]. The named systems are described in more detail in this chapter.

1.2 Coordinate system

The ATLAS results often reference ATLAS coordinates briefly described in this subsection. The origin of the right-handed coordinate system is placed at the IP with z-axis directed along the beam direction. This, in turn, defines the transverse x-y plane with x axis pointing towards the center of the LHC ring and y axis directed upwards. All transverse observables like p_T and E_T are defined in this 2D plane. Besides the mentioned Carthesian coordinates the asimuthal angle ϕ is defined in the transverse plane around the beam axis. Polar angle θ is the elevation angle measured from the beam axis. The following metric quantities are also to be mentioned:

- Pseudorapidity η = -ln tan(θ/2),
- Rapidity y = 1/2 ln [(E+p_z)/(E-p_z)]
- The distance between particles $\Delta R = \sqrt{\Delta\eta^2 + \Delta\phi^2}$

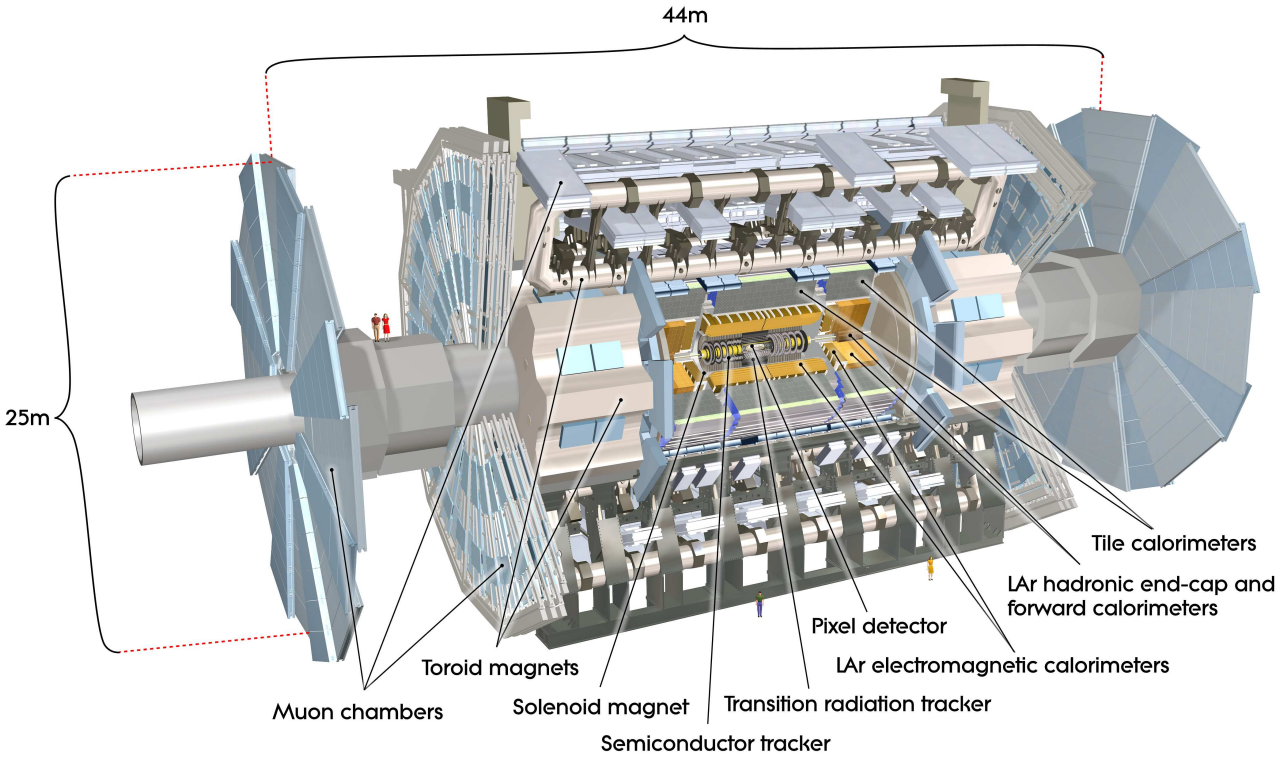

Figure 11: ATLAS detector general layout

1.3 Magnet system and magnetic field

ATLAS has a hybrid system of four supercoducting magnets which has 22 m in diameter, 26 m in length and stores an energy of 1.6 GJ [3]. The windings of the magnets are schematically shown in fig. 12. The four magnets that comprise the magnet system are the following:

- The central solenoid is aligned with the beam axis providing 2T axial magnetic field for the inner detector.
- A barrel toroid produces toroidal magnetic field of about 0.5T for the muon detectors in the barrel region.
- Two end-cap toroids produce toroidal magnetic field of approximately 1T for the muon detectors in the end-cap regions.

1.4 Inner detector

The ATLAS Inner Detector (ID) is designed to deliver pattern recognition, high-resolution momentum measurement [4],[5] along with primary and secondary vertex determination for charged particle tracks

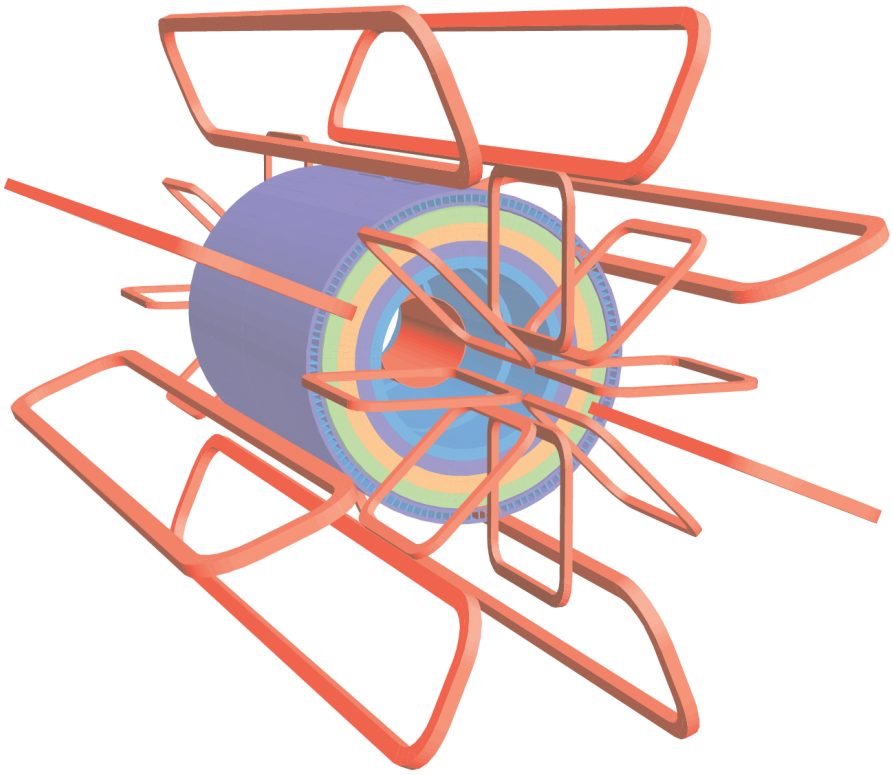

Figure 12: Geometry of ATLAS magnet windings

above a designated p_T threshold of 0.5 GeV (in some cases being capable of going as low as 0.1 GeV) within the pseudorapidity range $|\eta| < 2.5$. The inner detector provides reliable electron identification in rapidity range of $|\eta| < 2.0$ for energies from 0.5 GeV to 150 GeV.
The ID layout is a result of the technical requirements: it is assembled in a cylindrical envelope of 3512 mm in length and 1150 mm in radius. It is surrounded by the magnetic field of 2T imposed by the superconducting solenoid (see section 1.3).
Three independent sub-detectors complement each other in the inner detector (see fig. 18a (a)):

- Silicon pixel with 3 cylindrical layers for the barrel and 3 discs on each side for the end-cap. It provides the highest granularity around the vertex region. Normally each track hits three pixel layers. The pixel detector has about 80.4 million readout channels. Each of 1744 identical pixel sensors has 47232 pixels and 46080 readout channels. About 90% of the pixels have the size of 50x400 μm^2, the remaining pixels are a bit longer: 50x600 μm^2.

- Silicon microstrip layers (SCT) with 4 cylindrical layers and 9 discs on each side for the end-cap. A track typically crosses the strip layers in four space points. SCT has approximately 6.3 millions readout channels from its 15912 sensors. There are 768 active stripts of 12 cm lenght and 80 μm width per sensor plus two bias potential strips on the sensor edges.

- Transition radiation tracker (TRT) with 73 straw planes in the barrel and 160 straw planes in

the end-cap. The TRT has around 351,000 readout channels and detects in average 36 hits per track. The straw tubes that make up the TRT module are 4 mm thick and 1.44 m long (0.37 m in the endcap) and made out of polyamide films reinforced with carbon fibers. The straws are filled with gas mixture of 70% Xe, 27% CO_2 and 3%O_2 and supplied with gilded tungsten anodes which are directly connected to the readout channels. The pixel and SCT sensors are highly radiation-proof and operate in the temperature range from -5°C to -10°C to minimize the radiation damage, while the TRT module operates at room temperature.

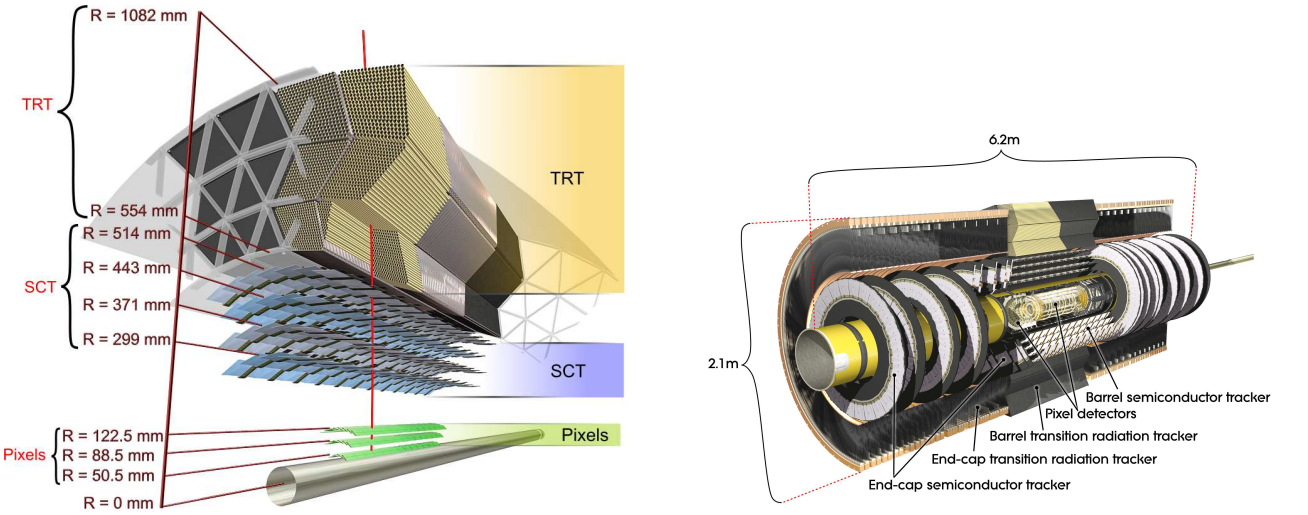

(a) Inner detector

(b) A perspective cut-away view of the pixel detector.

Figure 13: Fichier Gerber des modèles d CFR-34 et CFR-35.

1.5 Calorimeter system

The ATLAS calorimeter system covers the rapidity range within $|\eta| < 4.9$ and consists of several different detector systems. A rapidity region matched to the inner detector posesses fine granularity perfectly suited for high-precision measurements of photons and electrons. The remaining part's granularity is coarser but enough to perform jet reconstruction and measure E_T^{miss}. The view of ATLAS calorimeter is presented on fig. 15.

Besides measuring the energy of travelling particles calorimeters must also contain electromagnetic and hadronic showers, limiting their ability to go penetrate the calorimeter completely and get to the muon chambers. This provides a typical scale for size of the calorimeter modules: the EM calorimeter[6] is >22 radiation lengths (X_0) in the barrel and >24X_0 in the end-caps. The hadronic calorimeter has the thickness of 9.7 interaction lengths (λ) in the barrel and 10$\lambda$of in the endcap, which is enough to keep the leakage level below the typical muon background. This size also provides good resolution for the E_T^{miss} measuremet. The detailed description of the calorimeter system can be found in the table 11.

The tile calorimeter[7] uses scintillating tiles as active material alternated with steel absorbers. All the other calorimeter systems use liquid argon as an active medium with lead sampling.

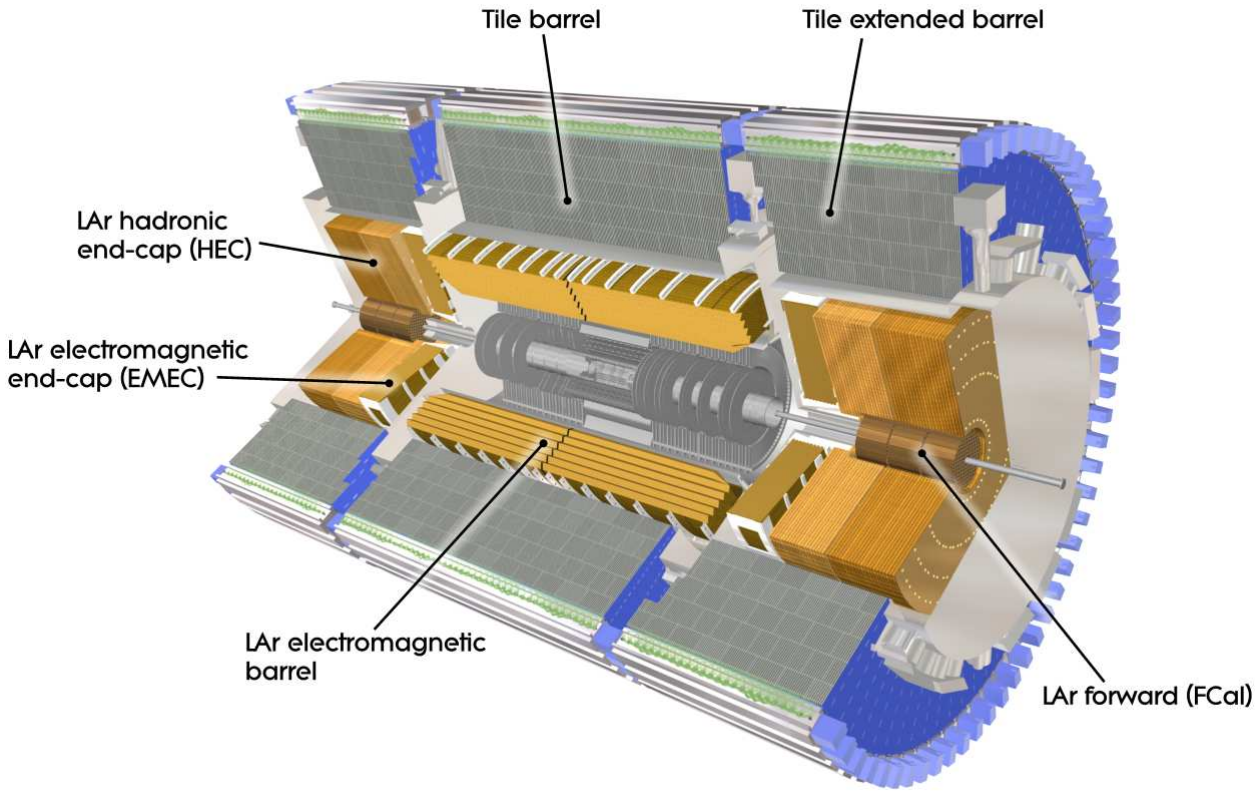

Figure 14: ATLAS calorimeter general layout

1.5.1 Electromagnetic calorimeter

The EMC has two submodules:

- EMC barrel detector.
- Electromagnetic end-cap calorimeter (EMEC) end-cap detector.

The EMC barrel module consists of two identical half-barrels 3.2 meters long with inner and outer radii 2.8 m and 4 m respectively. There is a 4mm gap at $z = 0$ between the half-barrels. The second crack is situated between the barrel and the end-cap at $1.37 < |\eta| < 1.52$. The EMEC comprises of two pairs of coaxial wheels of 63 cm thick having inner and outer radii of 330 mm and 2098 mm respectively. The crack between the two wheels makes a third crack at $|\eta| = 2.5$. Both barrel and end-cap electromagnetic calorimeters are designed to have an accordion-shaped absorbers made out of lead plates, coated in stainless steel sheets. The readout electrodes are placed in the gaps between the absorbers. This type

	Barrel	End-cap
EM Calorimeter		
Number of layers and $\|\eta\|$ coverage		
Presampler	1 $\|\eta\|$ <1.52	1 1.5 < $\|\eta\|$ <1.8
Calorimeter	3 $\|\eta\|$ <1.35	2 1.375 < $\|\eta\|$ <1.5
Granularity $\Delta\eta x\Delta\phi$ versus $\|\eta\|$		
Presampler	0.025×0.1 $\|\eta\|$ <1.52	0.025×0.1 1.5 < $\|\eta\|$ <1.8
Calorimeter 1st layer	0.025/8×0.1 $\|\eta\|$ <1.40	0.050×0.1 1.375 < $\|\eta\|$ <1.425
	0.025×0.025 1.425 < $\|\eta\|$ <1.5	0.025×0.1 1.425 < $\|\eta\|$ <1.5
		0.025/8×0.1 1.5 < $\|\eta\|$ <1.8
		0.025/6×0.1 1.8 < $\|\eta\|$ <2.0
		0.025/4×0.1 2.0 < $\|\eta\|$ <2.4
		0.025×0.1 2.4 < $\|\eta\|$ <2.5
		0.1×0.1 2.5 < $\|\eta\|$ <3.2
Calorimeter 2nd layer	0.025×0.025 $\|\eta\|$ <1.40	0.050×0.1 1.375 < $\|\eta\|$ <1.425
	0.075×0.025 1.4 < $\|\eta\|$ <1.475	0.025×0.025 1.425 < $\|\eta\|$ <2.5
		0.1×0.1 2.5 < $\|\eta\|$ <3.2
Calorimeter 3rd layer	0.050×0.025 $\|\eta\|$ <1.35	0.050×0.025 1.5 < $\|\eta\|$ <2.5
Number of readout channels		
Presampler	7808	1536 (both sides)
Calorimeter	101760	62208 (both sides)
LAr hadronic end-cap		
$\|\eta\|$ coverage		1.5 < $\|\eta\|$ <3.2
Number of layers		4
Granularity $\Delta\eta \times \Delta\phi$	0.1 × 0.1	1.5 < $\|\eta\|$ <2.5
	0.2 × 0.2	2.5 < $\|\eta\|$ <3.2
Readout channels		5632 (both sides)
LAr forward calorimeter		
$\|\eta\|$ coverage		3.1 < $\|\eta\|$ <4.9
Number of layers		3
Granularity $\Delta x \times \Delta y$		FCal 3.0 × 2.6 3.15 < $\|\eta\|$ <4.30
		FCal: ~four times finer 3.10 < $\|\eta\|$ <3.15
		4.30 < $\|\eta\|$ < 4.83
		FCal2 3.3 × 4.2 3.24 < $\|\eta\|$ <4.50
		FCal2: ~four times finer 3.20 < $\|\eta\|$ <3.24
		4.50 < $\|\eta\|$ < 4.81
		FCal3 5.4 × 4.7 3.32 < $\|\eta\|$ <4.60
		FCal3: ~four times finer 3.29 < $\|\eta\|$ <3.32
		4.60 < $\|\eta\|$ < 4.75
Readout channels		3524 (both sides)
Scintillator tile calorimeter		
	Barrel	Extended barel
$\|\eta\|$ coverage	$\|\eta\|$ < 1.0	0.8 < $\|\eta\|$ <1.7
Number of layers	3	3
Granularity $\Delta\eta \times \Delta\phi$	0.1 × 0.1	0.1 × 0.1
	0.2 × 0.2	0.2 × 0.1
Readout channels	5760	4092 (both sides)

Table 11: ATLAS calorimeter in numbers

of geometry allows full coverage in ϕ without cracks together with fast extraction of the signal from both sides of the electrodes. The orientation of the accordion waves is axial in the barrel and radial in the end-caps (see fig. 15). These features of the calorimeter lead to virtually uniform performace in ϕ dimension.

Segmentation in η is very different in the layers of the calorimeter, but the second layer always has the finest granularity because the egamma particles are supposed to leave most of their energy in the second calorimeter layer. In order to correct for the energy losses upstream the barrel calorimeter is preceded by a thin LAr active layer of 11mm thick called a presampler. For more details on η coverage and granularity see table 11.

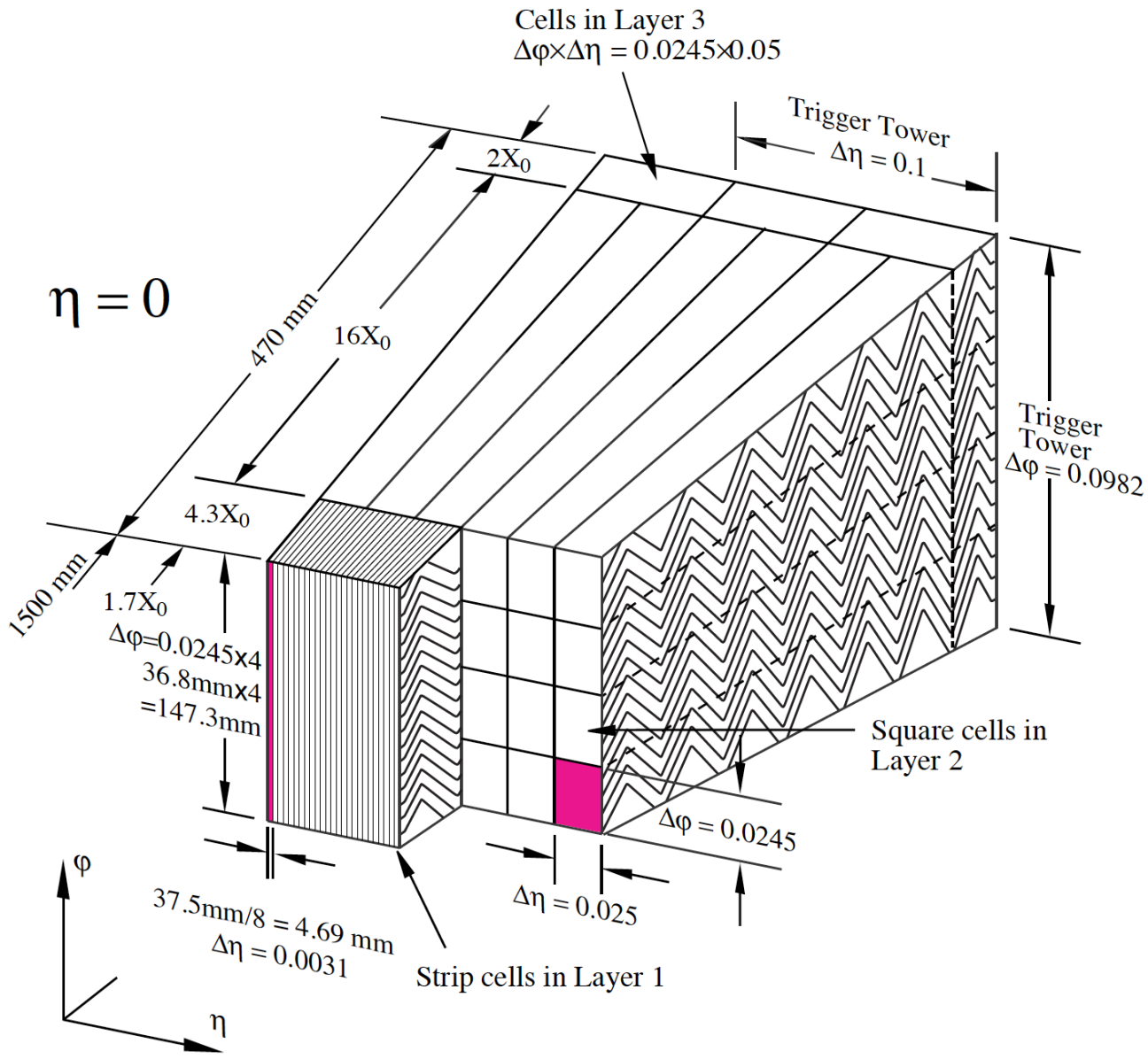

Figure 15: ATLAS EM calorimeter layers

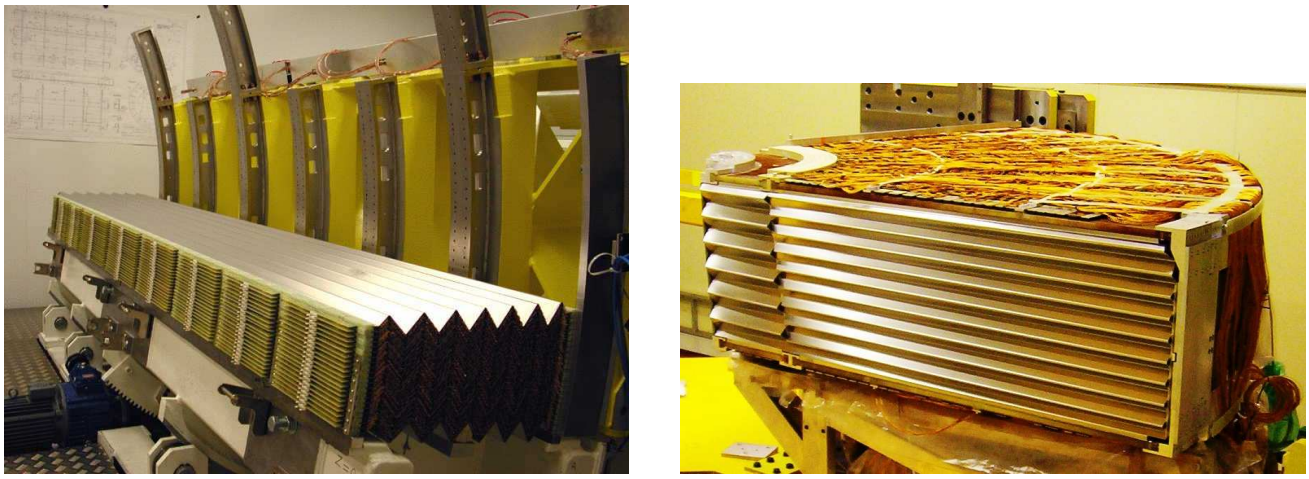

(a) Barrel **(b)** End-cap

Figure 16: Accordion absorbers of the EMC

1.5.2 Hadronic calorimeter

The hadronic calorimeter (HC) is combined of three submodules:

- HC scintilating tile detector, a steel sampled detector divided in turn into central barrel having 5.8 m in length and two extended barrels 2.6 m in length each. The extended barrels have inner radii of 2.28 m and outer radii of 4.25 m. The tile calorimeter consists of three layers having about 1.5, 4.1 and 1.8 interaction lengths λ in the barrel and 1.5, 2.6 and 3.3 λs in the extended barrel.

- Hadronic end-cap calorimeter (HEC) detector is a liquid argon calorimeter sampled with copper. It has two pairs of independent wheels symmetrically located behind the EMEC called the frona and the rear wheel. The wheels are cylindrical, their outer radius is 2030mm.

- Forward calorimeter (FCal) detector modules are located about 4.7 m from the IP and are subjected to very high particle flux and radiation. It consists of three wheels 45 cm deep each. The first one, FCal1 is sampled with copper intended for the measurement of electromagnetic processes. The two other wheels FCal2 and FCal3 are sampled with tungsted and designed for the hadronic showers measurement.

The number of the readout channels as well as the η coverage of every module and submodule is described in the Table 11.

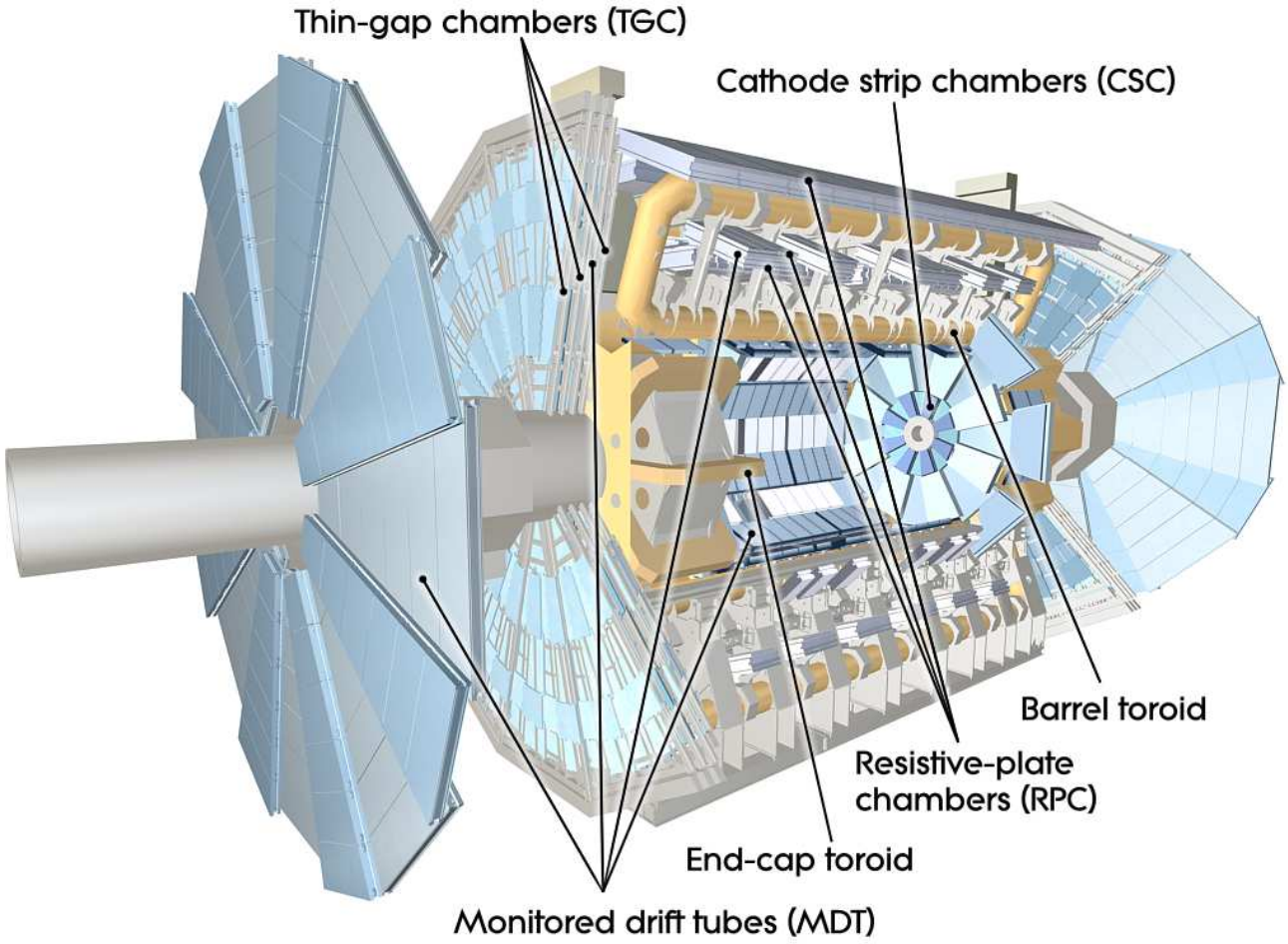

Figure 17: ATLAS muon system

1.6 Muon detectors

Most of the muons produced as a result of the p-p collisions are able to penetrate through calorimeters and make it to the muon detectors where their tracks are getting measured. The spectrometer provides high-precision measurement of the muon momenta in the rapidity range of $|\eta| < 2.7$ and approximate transverse momentum range of 3 GeV $< p_T <$ 3 TeV. The lower bound on the momentum is mainly due to energy losses in the calorimeter, while the upper bound is caused by the saggita bias coming from the tracking chambers alignment. The goal p_T resolution is about 10% for a 1 TeV muon track.
The muon tracks[8],[9] are bent by the torroid magnets allowing to determine muon kinematic properties. The large barrel toroid covers the rapidity range of $|\eta| < 1.4$, while at $1.6 < |\eta| < 2.7$ the tracks are bent by the smaller end-cap magnets. The deflection in the transition region of $1.4 < |\eta| < 1.6$ is provided by the barrel and end-cap fields combined.
The general layout of the muon spectrometer is depicted on fig. 17, the parameters of the muon systems can be found in table **??**. Just like the rest of the detector systems the muon spectrometer is split into

the barrel and the end-cap parts.
The muon spectrometer possesses a fast triggering system able to trigger for muons in the rapidity range of $|\eta| < 2.4$. It delivers the track information within a few tens of nanoseconds after the particle passage which also allows to use it for the bunch-crossing identification. The trigger chambers measure both η and ϕ coordinates of a track of which the former is in the bending plane and the latter is in the non-bending plane.
There are two types of fast triggering detectors used in the muon spectrometer:

- The Resistive Plate Chambers (RPCs) is a gaseous electrode-plate detector filled with a $C_2H_2F_4/Iso–C_4H_{10}/SF_6$ gas mixture (94.7/5/0.3). Two resistive plates of phenolic-melaminic plasctic laminate are separated by insulating spacers of 2 mm thickness. The plates contain an electric field of about 4.9 kV/mm such that the ionizing tracks cause avalanches towards the anode. The signal is read out through the capacitive coupling of metalic strips, mounted to the resistive plates. The RPCs have nominal operating voltage of 9.8 kV and provides an excellent time resolution of a few ns with a supported local rate capability of 1000 Hz/cm^2

- Thin Gap Chambers (TGCs) are multi-wire proportional chambers with the wire-to-cathode ditance of 1.4 mm and wire-to-wire distance of 1.8 mm and wire potential of 2900 V. The 2.8-mm gas gap is filled with highly quenching gas mixture of CO_2 and $n-C_5H_{12}$ (55/45). Small distance between the wires allows a very good time resolution of <25 ns in 99% of cases .

The precision-tracking chambers measure the coordinate of a track in the bending plane which is then matched with the second coordinate, measured by the trigger chamber.
There are two types of precision tracking systems used:

- The Monitored Drift Tubes (MDTs) are pressurised drift tubes with a diameter of 29.970 mm filled with Ar/CO_2 at 3 bar. Once the muon penetrates the tube it ionises the gas and the ionised electrons are collected at the central tungsten-renium wire of 50 μm in diameter and at a potential of 3080 V. This type of design carries several advantages: mechanical stiffness hence the alignment precision, reliability coming from the fact that a failure of a single tube would not cause malfunction of the others. MDTs counting rate is limited to 150 Hz/cm^2 which is not sufficient for the innermost layer in the forward region of $2.0 < |\eta| < 2.7$.

- Cathode Strip Chambers (CSCs) are gas detectors filled with Ar/CO_2 in 80/20 proportion. The ionised electrons are collected at the wires which are oriented in the radial direction and operate at a potential of 1900 V. They are installed in the so-called Small Wheels and there are 16 CSCs on either side of the ATLAS detector. . The CSCs are able to provide a countng rate of 1000 Hz/cm^2 which makes it a reasonable replacement for the MDTs in the region close to the beam.

The precision-tracking chambers in the barrel are positioned between and on the coils of the superconducting barrel thoroid magnet. They form three concentric cylindrical shells around the beam axis

at the approximate radii of 5 m, 7.5 m and 10 m. In the barrel region the RPCs were chosen for the fast triggering whereas the MDTs provide the precision tracking. The end-cap muon spectrometer is assembled in the form of large wheels perpendicular to the beam axis and located at distances about 7.4 m, 10.8 m, 14m and 21.5 m from the interaction point. The triggering in the end-cap is provided by the TGCs. Most of the precision tracking chambers are the MDTs similarly to the barrel, except for the forward region of $2.0 < |\eta| < 2.7$ where the CSCs are installed in the innermost tracking layer. The reason for that is their higher resistance to radiation and increased particle flow which becomes an issue if you get closer to the beam.

Barrel and end-cap alignment is illustrated on fig. 18which contains the side and transverse views of the muon spectrometer.

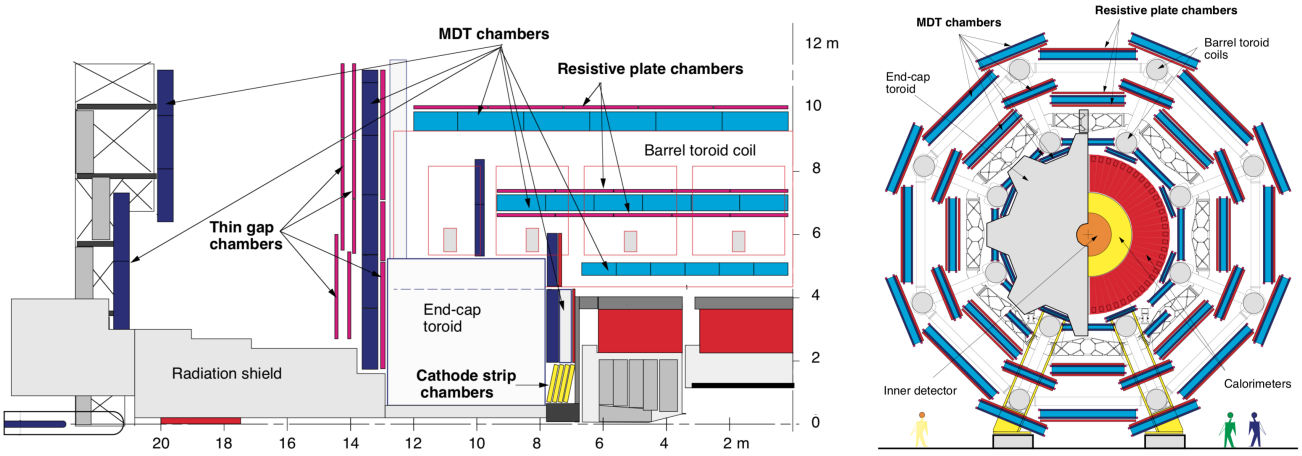

(a) Side view **(b)** Tranverse view

Figure 18: Cut views of the muon systems

1.7 Forward detectors

There are three detector systems that cover the ATLAS forward region (see fig. 19): LUminosity measurement using Cherenkov Integrating Detector (LUCID), Zero-Degree Calorimeter (ALFA) and Absolute Luminosity for ATLAS (ZDC). The measurement of luminosity if the main goal of the first two detectors and has fundamental importance: it provides the normalization scale for all the observed processes.

LUCID[10], [11] is the main ATLAS relative luminosity monitor. The main purpose of the LUCID detector is to detect inelastic p-p scattering in the forward region measuring the integrated luminosity and performing online monitoring of the instantenous luminosity and beam conditions with uncertainty of about few percent. It is symmetrically installed at ±17 m from the interaction point and at a radial distance of about 10 cm from the beam line (resulting in $|\eta| \approx 5.8$). On each side four bundles of quartz fibers are used as a medium producing Cherenkov radiation directing the Cherenkov light into the 16

Monitored drift tubes	**MDT**
Coverage	$\|\eta\| < 2.7$ (innermost layer: $\|\eta\| < 2.0$)
Number of chambers	1088 (1050)
Number of channels	339 000 (354 000)
Function	Precision tracking
Cathode strip chambers	**CSC**
Coverage	$2.0 < \|\eta\| < 2.7$
Number of chambers	32
Number of channels	31 000
Function	Precision tracking
Resistive plate chambers	**RPC**
Coverage	$\|\eta\| < 1.05$
Number of chambers	544 (606)
Number of channels	359 000 (373 000)
Function	Triggering, second coordinate
Thin gap chambers	**TGC**
Coverage	$1.05 < \|\eta\| < 2.7$
Number of chambers	3588
Number of channels	318 000
Function	Triggering, second coordinate

Table 12: ATLAS muon spectrometer subsystems coverage and parameters

Photomultiplicator Tubes (PMTs) placed outside the radiation shielding.
The ALFA[12] detector is used to measure the absolute luminosity through elastic scattering at small angles. In order to perform such measurement we need to meet the following conditions:

- The beam has to be more parallel than normally. Special collider beam optics allowing high values of the amplitude function at the interaction point $\beta*$ together with reduced beam emittance.
- To be sensitive to small angles the detectors have to be placed as far as possible from the interaction point and close to the beam. This is why the detectors are located inside the Roman pots at ±240 from the interaction point. On each side there are two Roman pots separared by four meters.

The Roman pot windows allow the elastically scattered protons reach the square scintillating fibres of 0.5 mm width which are in turn connected to multi-anode PMTs through the light-guides. The detector provides a spacial resolution of 30 μm and allows to measure absolute luminosity with uncertainty of 1.7% for the Run 2[13].
ZDC are used to detect forward neutrons at $|\eta| > 8.3$ in heavy-ion collisions, which in turn allows to determine the centrality of such collisions. The detector is installed at ±140 m from the interaction

point. Every ZDC arm consists of 4 modules: one electromagnetic and three hadronic. These modules are quartz rods shielded by the tungsten plates and connected to the PMTs via the light-guides allowing to measure incending particle energy and position. The EM module has a better position resolution mapping each of 96 quartz rods into a single pixel, while the hadronic modules map a bundle of four rods into a pixel. Only one of the three hadronic modules per arm provide position-sensing rods and only the arm at -140 m has the position-sensing EM module.

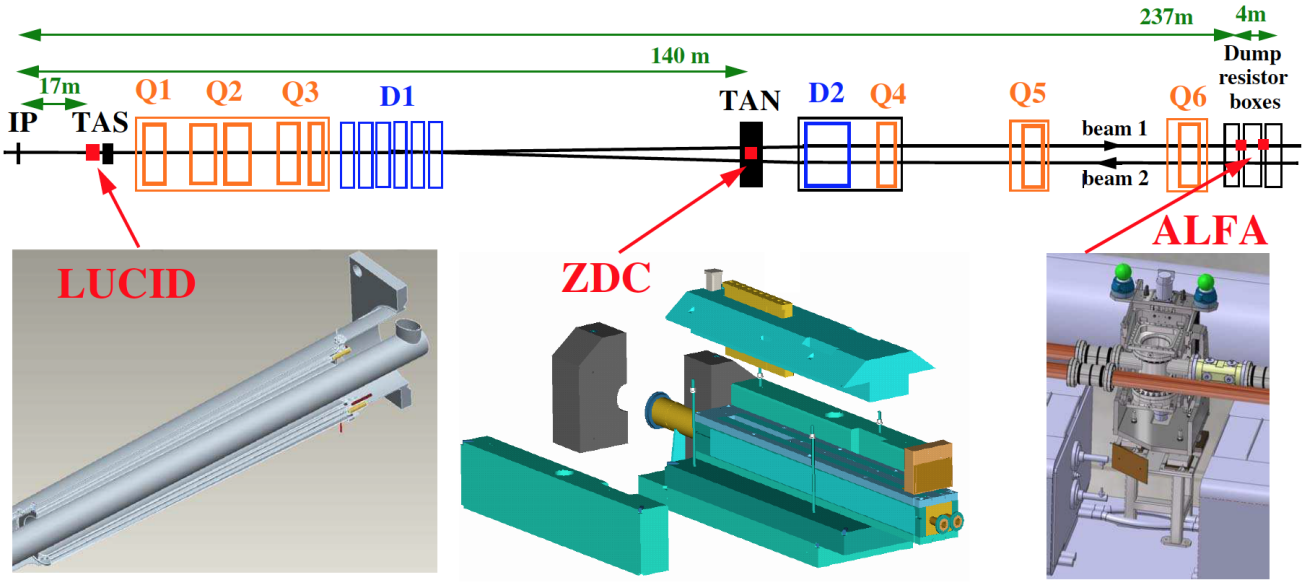

Figure 19: ATLAS forward detectors

1.8 Trigger system

Considering that the bunch crossing rate at LHC is about 40 MHz and that ATLAS detector has over one million read-out channels it would never be possible to store all the raw data without significant preselection that would decrease the data rate. The selection criteria are picked to retain and store only the events which might be interesting for the LHC physics. The preselection and storage is conducted with the help of TDAQ systems.

The trigger system has three distincs levels: L1, L2 and the event filter, the two latter levels are also called High-level Trigger (HLT). Each next level refines the decisions made before and, if necessary, applies additional selection, further lowering the event rate. The data acquisition system receives and buffers the event data from the readout electronics at the L1 trigger accept rate which for Run 2 is about 100 kHz [14]. The HLT then lowers the rate down to 1.5 kHz which is then stored for the offline analysis.

The L1 trigger looks for muons, electrons, photons, jets at handrons from τ-lepton decays with high transverse momentum, large missing and total transverse energy. The muons of interest are identified

using the muon spectrometer trigger system described in section 1.6. The rest of the particles are selected using the information from all the calorimeters with reduced granularity. During the Run 2 an intermediate L1Topo trigger was also added allowing to combine the information from the spectrometer and calorimeter and extend possible trigger selections. Results from these triggers gets processed by the central trigger processor which implements the trigger menu made up of different combinations of trigger selections. The decision latency for the L1 trigger must not exceed 2.5 μs after the corresponding bunch crossing.

For every selected event the L1 defines one or more regions called Region of Interest (RoI) which include the η and ϕ coordinates of these regions for their subsequent use by the HLT. The L2 selection is seeded RoI and uses full grnularity and precision along with other detector data available. The trigger block diagram is presented in fig. 110.

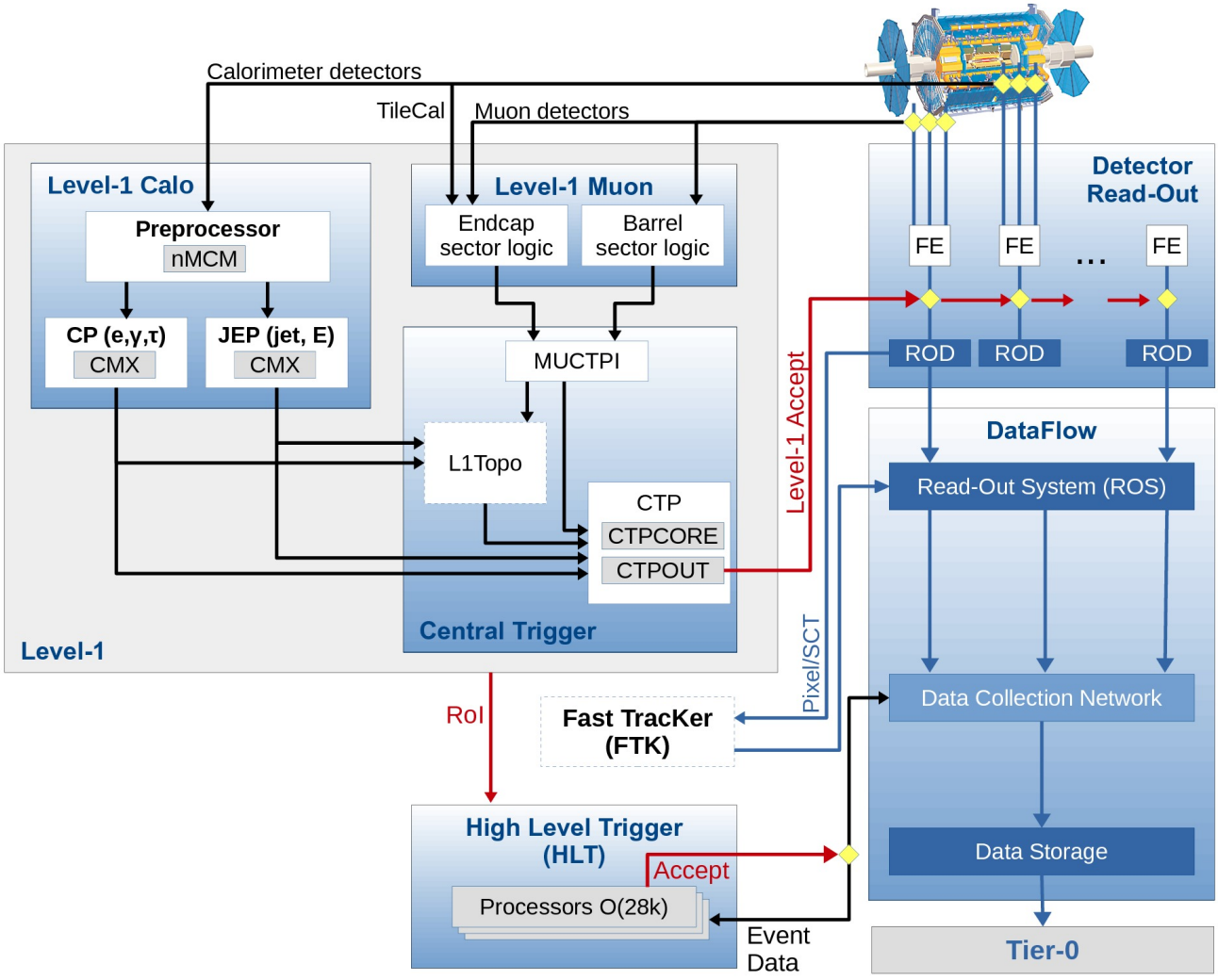

Figure 110: The scheme of ATLAS trigger systems

Bibliography

[1] G. Aad et al. "The ATLAS Experiment at the CERN Large Hadron Collider". In: *JINST* 3 (2008), S08003. DOI: 10.1088/1748-0221/3/08/S08003.

[2] Aranzazu Ruiz-Martinez and ATLAS Collaboration. *The Run-2 ATLAS Trigger System*. Tech. rep. ATL-DAQ-PROC-2016-003. Geneva: CERN, Feb. 2016. DOI: 10.1088/1742-6596/762/1/012003. URL: https://cds.cern.ch/record/2133909.

[3] *ATLAS magnet system: Technical Design Report, 1*. Technical Design Report ATLAS. Geneva: CERN, 1997. URL: https://cds.cern.ch/record/338080.

[4] *ATLAS inner detector: Technical Design Report, 1*. Technical Design Report ATLAS. Geneva: CERN, 1997. URL: https://cds.cern.ch/record/331063.

[5] S Haywood et al. *ATLAS inner detector: Technical Design Report, 2*. Technical Design Report ATLAS. Geneva: CERN, 1997. URL: http://cds.cern.ch/record/331064.

[6] *ATLAS liquid-argon calorimeter: Technical Design Report*. Technical Design Report ATLAS. Geneva: CERN, 1996. URL: https://cds.cern.ch/record/331061.

[7] *ATLAS tile calorimeter: Technical Design Report*. Technical Design Report ATLAS. Geneva: CERN, 1996. URL: https://cds.cern.ch/record/331062.

[8] *ATLAS muon spectrometer: Technical Design Report*. Technical Design Report ATLAS. Geneva: CERN, 1997. URL: https://cds.cern.ch/record/331068.

[9] ATLAS Collaboration. *Technical Design Report for the Phase-II Upgrade of the ATLAS Muon Spectrometer*. Tech. rep. CERN-LHCC-2017-017. ATLAS-TDR-026. Geneva: CERN, Sept. 2017. URL: https://cds.cern.ch/record/2285580.

[10] g chiodini g, n orlando n, and s spagnolo s. *ATLAS RPC time-of-flight performance*. Tech. rep. ATL-MUON-PROC-2012-002. Geneva: CERN, Apr. 2012. URL: https://cds.cern.ch/record/1437020.

[11] Marco Bruschi. *The new ATLAS/LUCID detector*. Tech. rep. ATL-FWD-PROC-2015-002. Geneva: CERN, June 2015. URL: https://cds.cern.ch/record/2025000.

[12] S. Abdel Khalek et al. "The ALFA Roman Pot Detectors of ATLAS". In: *JINST* 11.11 (2016), P11013. DOI: 10.1088/1748-0221/11/11/P11013. arXiv: 1609.00249 [physics.ins-det].

[13] *Luminosity determination in pp collisions at $\sqrt{s} = 13$ TeV using the ATLAS detector at the LHC*. Tech. rep. ATLAS-CONF-2019-021. Geneva: CERN, June 2019. URL: https://cds.cern.ch/record/2677054.

[14] William Panduro Vazquez and ATLAS Collaboration. *The ATLAS Data Acquisition system in LHC Run 2*. Tech. rep. ATL-DAQ-PROC-2017-007. 3. Geneva: CERN, Feb. 2017. DOI: 10.1088/1742-6596/898/3/032017. URL: https://cds.cern.ch/record/2244345.